Temperature and velocity fields in natural convection by PIV and LIF

Knud Erik Meyer, Poul S. Larsen
Department of Mechanical Engineering, Fluid Mechanics Section
Technical University of Denmark, Building 403, DK-2800 Lyngby, kem@mek.dtu.dk

Fabrice Guillard and Carsten H.Westergaard
Dantec Dynamics A/S
Tonsbakken 16-18, DK-2740 Skovlunde, Denmark

ABSTRACT

Natural convection in a cubical cavity (L = 250 mm) filled with water is created by heating a square plate (0.5 L) centred in the bottom wall and by cooling the sidewalls, while the remaining walls are insulated. The Rayleigh number based on cavity side length and temperature difference between plate and cooled walls is $1.4 \cdot 10^{10}$. The flow is turbulent and is similar to some indoor room flows. Combined Particle Image Velocimetry (PIV) and Planar Light Induced Fluorescence (LIF) are used to measure local velocities and temperatures. Data measured in a symmetry plane parallel to a sidewall are presented in terms of mean velocities and temperature and in terms turbulent quantities including Reynolds fluxes. The flow consists a plume rising above the heated plate into an almost stagnant fluid with a weakly stratified temperature field, as well as thin buoyancy driven boundary layers down the sidewalls. The measured Reynolds fluxes show that the dominating heat transport is in the plume in vertical direction. This transport relates to hot parcels of fluid rising due to buoyancy. A considerable heat transport in horizontal direction from the plume to the surrounding, stagnant fluid maintains the stratified temperature field.

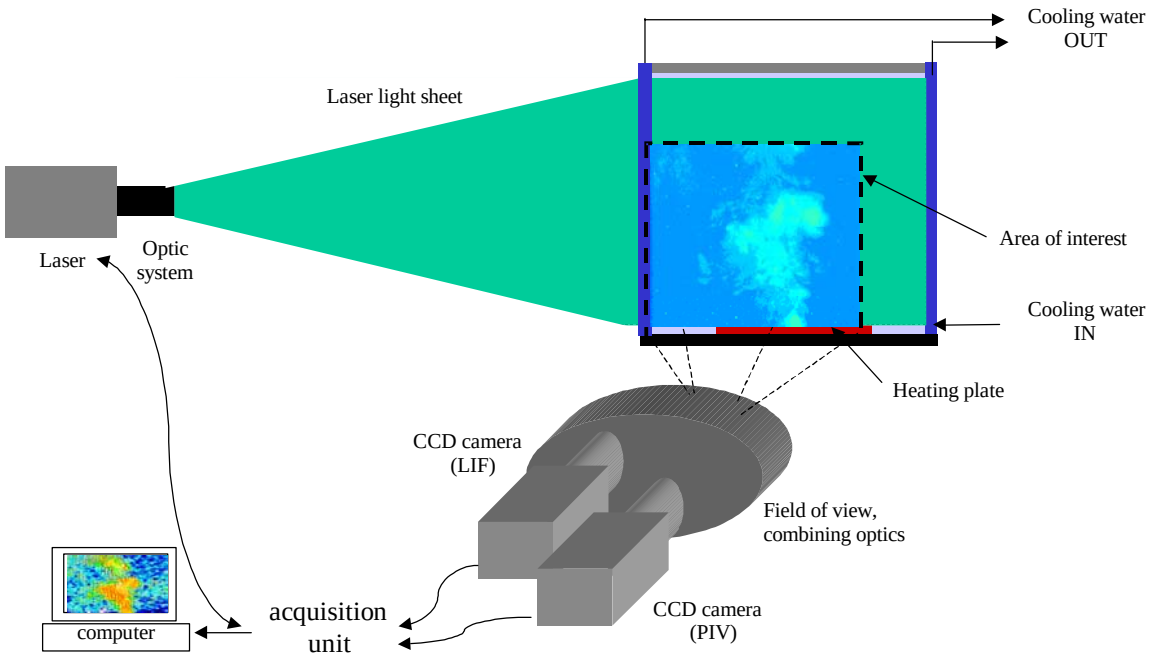

Fig. 1. Schematic diagram of the experimental PIV/planar-LIF installation

1. INTRODUCTION

Natural convection plays an important role for the comfort of a person in a room. Flows created by temperature differences near a person or near a cold wall are characterized by Rayleigh numbers of the order of 10^9, which implies turbulent flow. However, in zones of the room with low velocity, the flow can also feature laminar flow patterns. Such flows are difficult to simulate accurately with numerical methods and require experimental characterization, using non-intrusive methods. The application aspect of the present study is to investigate details of such flows experimentally. The results can give insight into the dynamics of these buoyancy driven flows and can also be used to understand the relative importance of different terms in turbulence models.

The most common configuration for natural convection model studies in a box is to have one sidewall heated, the opposite wall cooled and the remaining boundaries thermally insulated. A recent experiment of this type has been presented by Leong *et al*. (1999). The present configuration, however, considers the more general and complex model problem of a cubical cavity with a heated surface at the centre of the bottom wall, with cooling of the sidewalls and with the top wall thermally insulated. The heated plate and the cooled walls are designed to have approximately uniform temperatures, and the problem thus involves both confined plume and vertical boundary layers, which present a considerable challenge to three-dimensional numerical simulation in a simple geometry.

In the present work planar laser induced fluorescence synchronized with PIV is used simultaneously to investigate both temperature and flow fields. It has been demonstrated e.g. by Coolen *et al*. (1999) and Seuntiëns *et al*. (2001) that accurate measurements of the local temperature in water can be made with laser-induced fluorescence (LIF). This approach uses a frequency doubled, pulsed Nd:YAG laser and CCD-camera as employed by common Particle Image Velocimetry (PIV) systems. The present study uses the same for the temperature measurements, however combined with simultaneous PIV measurements of local velocities to give also turbulent quantities like Reynolds fluxes. The present work is a continuation of the work presented by Meyer *et al*. (2000) where Reynolds fluxes of mass transfer were measured with a combined PIV/planar-LIF system, the passive scalar being a concentration.

Section 2 describes the experimental set-up used to carry out PIV/Planar-LIF measurements. Section 3 gives the details including the technical limitations of the measurement methodology, as well as the optimisation methods implemented. Here, special attention is given to calibration, including the design of a general procedure of how to 'seed' a given flow with fluorescence tracer and how to determine the temperature resolution and absolute accuracy of the measurements. Section 4 presents the results and the discussions of the velocity/temperature measurements in the cavity.

2. EXPERIMENTAL METHOD

2.1 Flow equipment

Figure 2 shows a sketch of the experimental flow setup and defines the coordinate system used. The cavity has a side length of L = 250 mm and is filled with tap water. The four double sidewalls of the cavity each consist of an inner wall of 2 mm glass plate and an outer wall of 5 mm glass plate. Cooling water is circulated in the 2 mm slit between the two glass plates at the four sides. The mean velocity of this water flow is larger than 0.5 m/s and the heat transfer between the inner wall and the cooling water is therefore high. The temperature difference between inlet and outlet of the cooling water is less than 0.5 K. It is therefore assumed that the temperature of outer surface of the inner wall is uniform and equal to the temperature of the cooling water. The bottom wall (outside the heated block) and the top wall are made of 5 mm acrylic plate and are assumed to act as insulated surfaces.

In the bottom wall, an electrically heated square aluminium block is inserted at the centre. The aluminium block has a side length of 0.5 L = 125 mm and a thickness of 16 mm. The block contains three cylindrical electrical heater elements that each has a diameter of 6.5 mm and a length of 100 mm. The heaters are placed in parallel with a horizontal distance of 42 mm between the centrelines and are located symmetrically with respect to the horizontal symmetry lines in the block. The distance from the top of the block to heater centrelines is 10 mm. The block is equipped with three thermocouples mounted just below the top surface: one at the centre of the block, one between horizontal positions of two heaters, and the last one at a corner at a distance of 10 mm from both side walls. During the measurements the two first thermocouples showed the same temperature within 0.3 K. Their mean temperature is used for the hot surface temperature. However, the thermocouple at the corner showed a temperature of up to 7 K below those of the other thermocouples. This indicates that the temperature was constant over the main part of the block, but that due to the

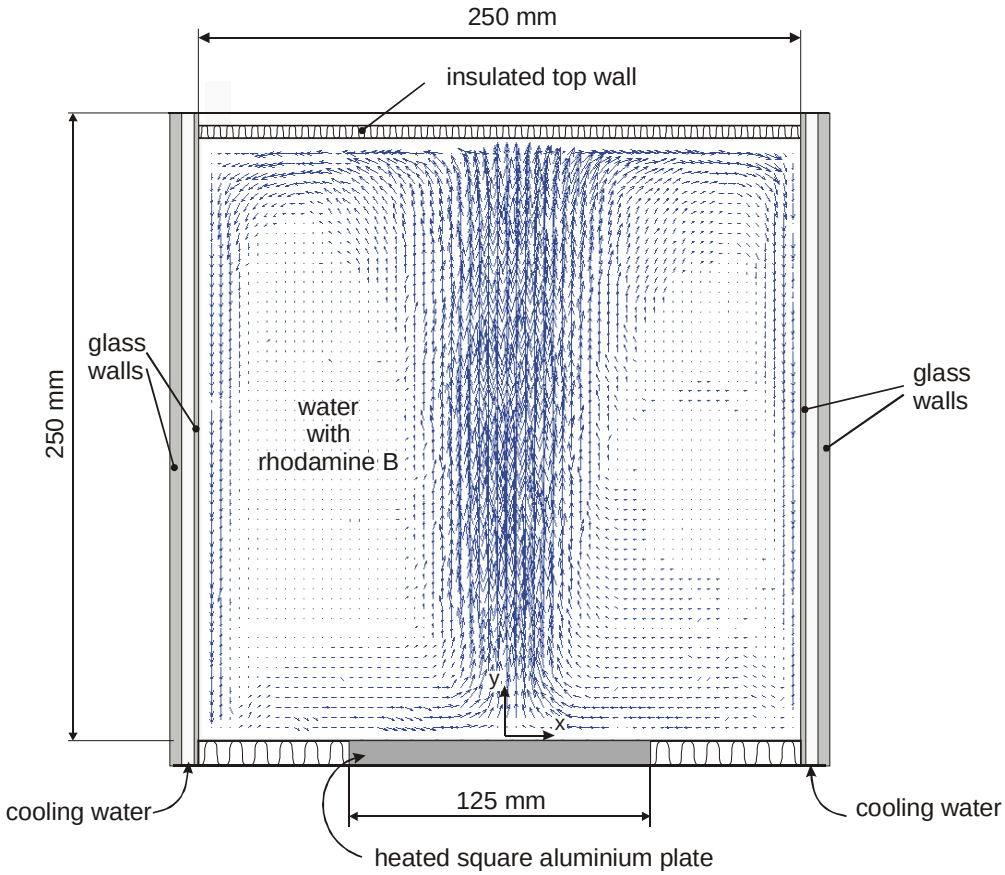

Fig. 2. Cross section of experimental cubical cavity with coordinate system (schematic) and mean velocity vectors of the resulting flow in the full plane of symmetry parallel to a sidewall.

absence of local heating at the edges and probably also high heat transfer since boundary layers start here, the temperature decreases close the edges of the block.

To a first approximation the cavity can be considered to satisfy the boundary conditions of constant temperatures at the heated plane and the cooled walls. An accurate description of the thermal boundary conditions should include heat conduction in the aluminium block and in the inner glass walls.

2.2 PIV/Planar-LIF equipment

A schematic drawing of the experimental setup to implement PIV/temperature planar-LIF measurements is shown in figure. 1. The Nd:YAG laser (NewWave Solo, 50 mJ, double cavity) provides a beam of green light, which is passed through optics to produce a thin sheet with measured thickness D_z = 4 mm (i.e. 0.016×L). This light sheet is positioned to illuminate the whole mid-section of the cavity parallel to a sidewall. Two Dantec HiSense CCD cameras (1280×1024 pixels, 12 bit) with Nikor 60mm lenses are used to view the lower part of the cavity. Both cameras were operated in binned mode, where 2x2 pixels are read electronically from the camera head as one pixel, increasing the signal to noise ratio on the camera CCD, but lowering the resolution to 640 x 512 pixels. The camera that records the scattered light is equipped with a 3 nm narrow-band filter at 532 nm and operates in PIV cross-correlation mode. The second camera, which captures the fluorescence signal, is equipped with an orange 560 nm low-pass cut-off filter to avoid scattered light from particles entering the detector. These cameras are fitted into a Dantec two-camera mount for optical pre-alignment and hence view the same area with same spatial resolution (0.345 mm/pixel; i.e. D_x, D_y = 0.0014×L ≈ 0.1 D_z with D denoting spatial resolution). Fine alignment is obtained using a geometric calibration. The calibration map is later used to re-sample the LIF-images with the spatial coordinate of the PIV-camera ensuring maximum correlation between velocities and temperature, which is important for Reynolds flux calculation.

2.3 Measurement methodology

2.3.1 PIV measurements

Small polyamid spheres with mean diameter of 20 μm and density at 1.03 g/cm^3 are added to the water in the cavity. The seeding is adjusted so that the number of particles per interrogation area is (i) high enough to ensure accurate measurements of particles displacement and hence velocity calculations and (ii) sufficiently low to ensure that the local fluorescence signal caused by light scatter from the particles is insignificant.

2.3.2 Planar-LIF calibration procedure

A solution of Rhodamine B is used as fluorescence tracer during these preliminary experiments. The concentration is chosen so as to get the maximum signal at room temperature, keeping the absorption levels sufficiently low so that the linear regime approximation is valid while temperature resolution and temperature range are optimal. The calibration procedure developed in this work is described in section 3.

2.3.3 Image processing

PIV-images are processed using interrogation areas of size 16×16 pixels with 50% overlapping in each direction giving 79×63 velocity vectors. The processing employed adaptive correlation using a forward difference scheme and a 3×3 local neighbourhood validation. LIF-images are transformed into temperature fields according to (1). In this equation, S denotes the instant fluorescence recorded at the position (x,y) and $\overline{S^{\mathrm{Ref}}}$ is the reference signal for $T_{\mathrm{Ref}} = 0$°C. This value is statistically determined over 6 different temperature levels where each temperature level is based on 9 to 14 images. The coefficient $\overline{\alpha}$ is also statistically determined during calibration and refers to the precision of the measurements (see section 3.1).

$$T_{(x,y),t} = \left(\frac{S_{(x,y),t} - \overline{S^{\mathrm{Ref}}_{(x,y)}}}{\overline{\alpha_{(x,y)}}} \right) \qquad (1)$$

3. SET-UP OPTIMIZATION

In order to ensure an optimal LIF signal the following needs to be considered:

(i) Low signal-to-noise ratio (SNR) inherent to the methodology used; i.e. the liquid is homogeneously seeded with the marker, whose fluorescence signal is proportional to the local temperature by a factor of only 1.5-2 %/°C.
(ii) Low fluid temperature variation (only about 5°C between the temperature near the plate and the surrounding fluid)
(iii) Large imaging area (200×160 mm), giving low illumination hence requiring high marker concentration, and large penetration depth (125 mm), demanding low marker concentration to minimize absorption.

3.1 Defining the optimal concentration level

Temperature measurements are based on the change of quantum efficiency of the dye with local temperature. As the sensitivity of Rhodamine B to temperature is of the order of 2-3% per °C, the initial interrogation is to determine at which concentration the water in the cavity must be seeded to yield the highest temperature resolution possible. The general methodology is implemented to find the optimal concentration (C_{opt}) without running a series of trials. This methodology consists in calibrating the system with respect to temperature at various concentration levels (figure 3) and relating the results to absorption phenomena (figure 4). This preliminary step is carried out in a smaller cavity before running final calibration and experiments in the actual model cavity.

The temperature resolution R, defined as the inverse of the slope of the curve 'Grey-level vs. Temperature' gives the precision on the measurements (the lower the value of R, the better the precision becomes). Naturally, the objective is to set-up the system to get the best precision possible so as to capture small spatial gradients in temperature. In figure 4 (top), the temperature resolution for a given position is plotted at various concentrations C_o. As is expected, the resolution is mediocre at low C_o-values (e.g. R = 2°C/GreyLevel at C_o ~ 1 μg/l). When increasing C_o, R asymptotically approaches a minimum (R_{min} ~ 0.21°C/GreyLevel at C_o ~ 13.5 μg/l) and then increases again. The concentration R_{min}

represents the optimal concentration. As can be seen in figure 4 (bottom), this concentration also corresponds to the concentration level at which the absorption calculated from (2) becomes significant; e.g. $A \approx 0.08$ for very accurate concentration measurements (see Guillard *et al.*, 2000).

$$A = \exp[- (\Sigma l)\, \varepsilon_{Rhod}\, C_0] \quad . \tag{2}$$

where ε_{Rhod} is the extinction coefficient of Rhodamine B in water and Σl the optical path length.

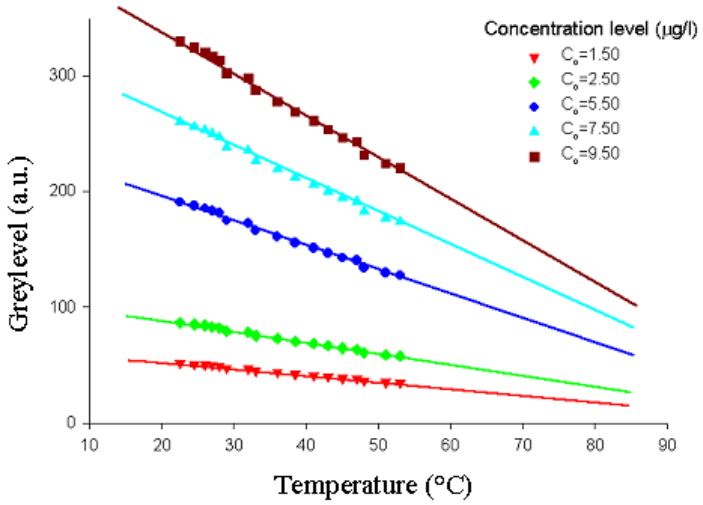

Fig. 3. Single-pixel temperature calibration curves at various levels of concentration. Small cavity tests.

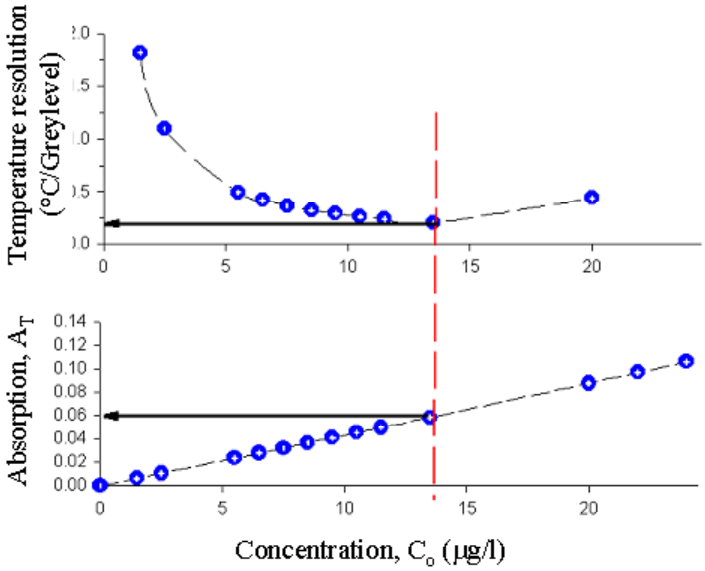

Fig. 4. Precision of (single-pixel) temperature calibration as a function of the concentration in terms of resolution (upper) and absorption (lower) versus concentration. Small cavity tests.

According to these findings, calibration must be performed in two steps. First, small amounts of dye are added so as to build a reference calibration map that indicates at which concentration the system becomes saturated ($C = C_{max}$, as described by the (red) vertical dashed line in figure 4). Here, the temperature dependency of Rhodamine B is not significant since only semi-quantitative information is required. Once the maximum concentration is determined, the

cavity is seeded with Rhodamine B at a concentration of $C \approx 0.9 \times C_{max}$ and the final calibration of intensity versus temperature can be performed.

3.2 Precision and accuracy of the measuring technique

Precision and accuracy of the measurements (in the cavity) are quantified at four randomly selected positions (pixels) in the cavity based on 9 – 14 images recorded at each of a number of constant water temperature levels and extrapolated to the whole image area. The results of the precision analysis are reported in Table 1. One finds that the overall temperature resolution (R) over the four positions is stable around the value of 0.02°C/GreyLevel.

Table 1 - Statistical analysis of the calibration: Precision analysis.

Position	**P1**	**P2**	**P3**	**P4**
Temperature resolution (R)	0.0209	0.0187	0.0198	0.0174
Regression coefficient (r^2)	0.9990	0.9960	0.9978	0.9860

Defining the accuracy by the 95% confidence limit and taking the same four positions to represent the whole field, one finds an average absolute error of the order of 0.66°C (Table 2) based on (3), where t denotes the factor from Student's t-distribution. Moreover, no obvious pattern between the error amplitude and the temperature is observed.

$$\varepsilon_T = t_{n-1}^{0.05} \frac{Rms(T)}{\sqrt{n-1}} \tag{3}$$

Table 2 - Statistical analysis of the calibration: Error analysis.

Temperature (°C)		**36.6**	**34.4**	**29.5**	**27.0**	**23.2**	**20.6**
Error level, ε_T (°C)	P1	0.45	0.55	0.84	0.64	0.63	1.03
	P2	0.67	0.44	0.77	0.72	0.29	0.93
	P3	0.47	0.92	0.91	0.33	0.95	0.68
	P4	0.74	0.54	0.63	0.75	0.59	0.69

As indicated by the temperature error analysis given in table 2, the fluctuation from image to image is fairly significant. These fluctuations are due to several factors, but primarily variation in the light sheet from laser pulse to laser pulse. The light intensity of the laser varies, but also the shape of the laser beam profile varies. Both are revealed in figure 6, which shows vertical profiles (row averaged over 100 pixels) of grey levels in five successive calibration images. The mean values of all pixel used for each image are also shown in figure 6 (by +), having a variation that is significantly lower than the local variation. In Meyer *et al.* (2000), the variation in the light intensity was corrected in each image by selecting a region of know fluorescent intensity and normalising with that value. Seuntiëns *et al.* (2001) used a similar technique. In the present experiment this was not possible. The peak-to-peak value of the local intensity fluctuation is about 100 grey levels, or about 2°C.

Secondly, it can be seen that even if the five profiles in figure 6 were normalised, there is a small slope difference. This is, at least partially, due to shape changes of the laser beam profile from pulse to pulse. These variations are also revealed in figure 5, showing some slowly varying temperature in profiles perpendicular to the light propagation. The order of magnitude here is about the same as the total light intensity variation. In summation, the fluorescent signal from the temperature fluctuation in this experiment is rather low. Correcting for laser intensity fluctuations would help, but cross-section correction would also be required in order to obtain standard deviation of temperature at correct levels. Seuntiëns *et al.* (2001) were able to make such a correction because a large portion of their images contained a constant, known temperature.

The calibration procedure and optimisation methods defined here led to a significant enhancement of the signal-to-noise ratio, rendering whole-field temperature measurement possible with a precision of 0.02°C/GreyLevel and an absolute accuracy of 0.6°C on mean temperature maps. It should be noted that the accuracy on instantaneous temperature maps is somewhat poorer (up to 2°), as explained above, meaning that the standard deviation of temperature is not a reliable measure. When comparing the performance of the present set-up to previous works (Table 3), one finds that the material and methods used here gives results among the best reported in the literature.

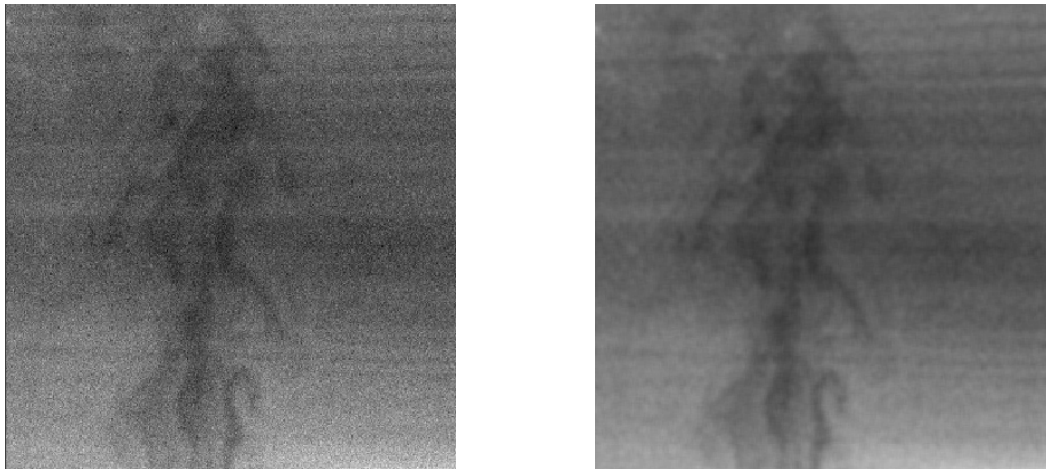

Fig. 5. Typical instant temperature maps raw image (left) and the same image with morphology correction (right).

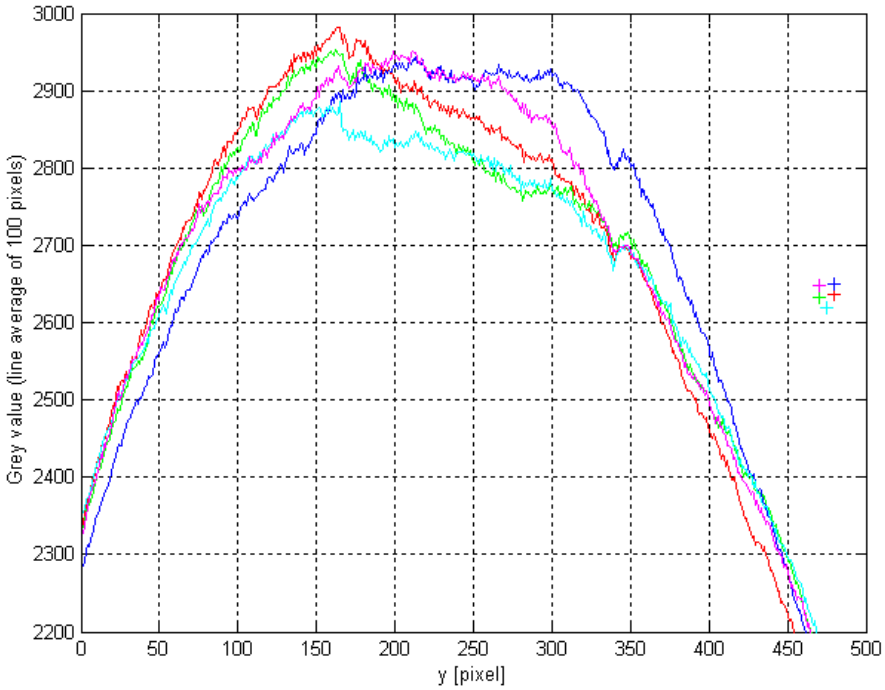

Fig. 6 . Mean value of rows of first 100 horizontal pixels in each image line versus vertical pixel position for five consecutive images taken at one uniform water temperature of 23.2°C. The symbol + (to the right) denotes the mean value of each curve of corresponding colour.

Table. 3 - Performance comparison of various temperature planar-LIF systems.

Reference	**Temperature resolution**	**Error level (95% interval limit)**	**Comments**
Mahouast (1993)	1°C/GreyLevel	Not reported	8 bit camera
Coolen *et al.* (1999)	0.02°C/GreyLevel	1.7°C	8 bit camera Adimec MX12
Seuntiëns *et al.* (2001)	0.4°C/GreyLevel	0.1°C	8 bit camera Kodak ES 1.0
Present study	0.02°C/GreyLevel	0.6°C	12 bit camera HiSense

3.3 Optimising instant temperature map by image post-processing

In figure 5 (left), the instant temperature map shown reveals a somewhat noisy background with some temperature variations from pixel-to-pixel. This is inherent to the (resolution, accuracy)-values obtained; namely $R << \varepsilon_T$. To numerically reduce the effect of recording noise, a morphology filter is applied to all instant temperature maps. As observed in figure 5 (right), this post-processing significantly reduces the pixel-to-pixel noise and lead to enhanced quality of the temperature map, but giving a slight reduction of the spatial resolution.

4. RESULTS AND DISCUSSION

Experimental results are presented for one test case of a thermal plume in a box driven by a square heat plate at the bottom of the box. The measured velocity and temperature fields are based on 5000 PIV/PLIF samples taken at 1 Hz. This sample rate cannot resolve the typical turbulent velocity fluctuations in the flow but does resolve the global unsteady flow phenomena having a time scale significantly larger than one second. Therefore, the samples cannot be claimed to be completely uncorrelated, yet the total series of 5000 samples still corresponds to several hundred statistically independent samples. The coordinate system used in the presentation has origo at the centre of the heated plate with a horizontal x-axis (perpendicular to a sidewall) and a vertical y-axis (perpendicular to the heated plate) as shown in figure 2.

4.1 Heat transfer conditions

During the experiment the power supply to the heated plate was kept constant at 433 W and the cooling water was kept at 19.0±0.5°C. After more than an hour of stabilization, the temperature of the centre of the heat plate was measured to be 60.0°C. A Nusselt number Nu (based on total heat power, total temperature difference, and plate side length) was found to be 66% of the value predicted by the correlation for free convection from a horizontal plate: $Nu = 0.15\ Ra^{1/3}$ (Incropera and DeWitt, 1985), Ra being the Rayleigh number. The heat transfer from the heat plate is therefore limited by the stratified temperature field and the presence of walls. The Rayleigh number based on the cavity side length was $Ra = 1.4 \cdot 10^{10}$.

4.2 Mean velocity and temperature

An overview of the developed mean flow is shown in figure 2 as velocity vectors from a preliminary measurement covering the full mid plane of the cavity. Final results of mean velocity vectors from the 5000 samples are shown in figure 7, indicating tht the flow is dominated by a plume rising above the heated plate. The fluid at the sides of the plume has almost no velocity. Thin boundary layers with downward flow are found at the sidewalls. These boundary layers are not resolved in detail in the present measurements. Figure 7 also shows contours of mean temperature indicating a stratified temperature distribution with temperatures of about 20°C at the bottom (almost equal to the sidewall temperature) and about 30°C at the top.

Figure 8 shows line profiles for different variables at different constant y-values. The plot of vertical mean velocity V shows the expected bell shaped velocity profile of the plume. At $y/L = 0.1$, the velocity profile is relatively narrow and is still not fully developed. Profiles for y/L = 0.3, 0.5 and 0.7 have similar maximum velocities and widths. For y/L = 0.7, slightly negative V-velocities are found at the edges of the plume. This indicates the presence of large vortices near the top of the cavity.

The mean temperature profiles show a peak above the heated plate for y/L = 0.1, 0.3 and 0.5, but no peak for y/L = 0.7, but otherwise a stable thermal stratification with temperature increasing with height y/L throughout the cavity. The stable stratification explains the vanishing velocities in the bulk outside plume and wall boundary layers. It is interesting to note that the increase in mean temperature at x = 0 ceases at about y/L = 0.7 where the effect of the top wall seems to control the temperature field. At y/L = 0.1 both velocity and temperature profiles are slightly asymmetric, maximum velocity and temperature being found at y/L = 0.02 and temperature for $x > 0$ being slightly lower than for $x < 0$. It has not been possible to determine the reason for this asymmetry.

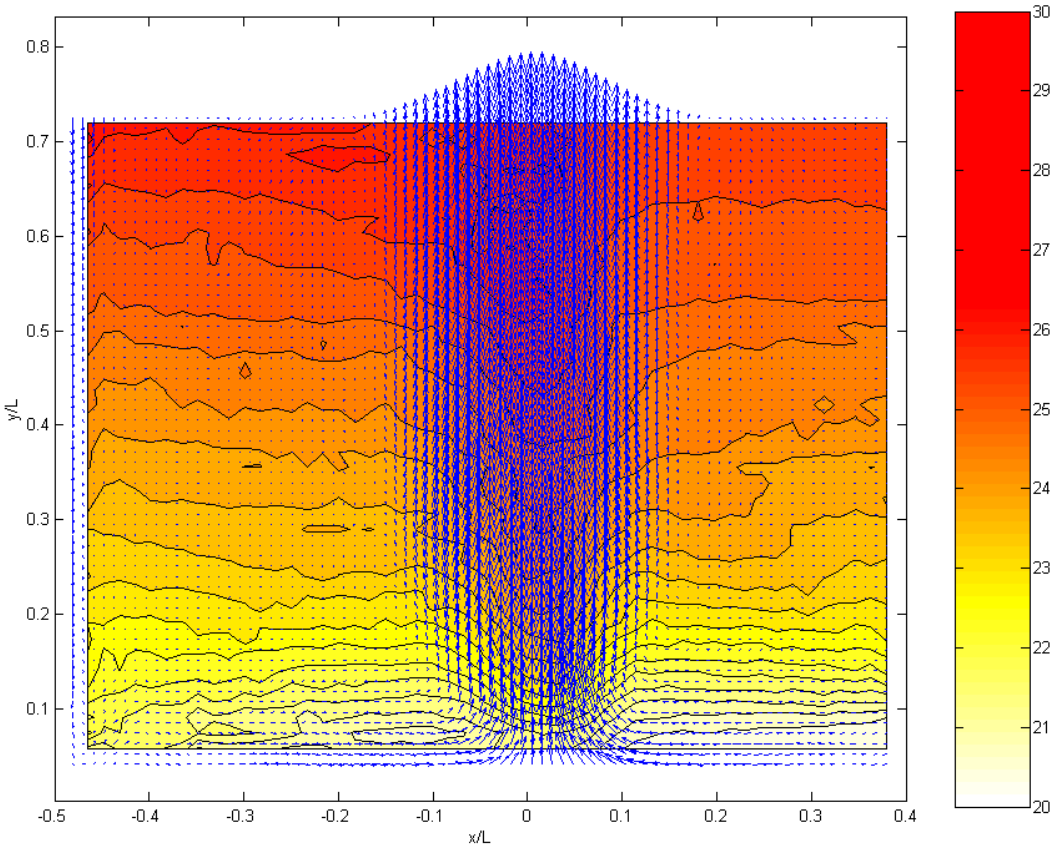

Fig. 7. Contours of the mean temperature and vectors of mean velocity. Colormap show temperature in °C.

4.3 Turbulent quantities

Figure 8 also shows the standard deviation (RMS-value) of the vertical velocity component std(V) and the temperature std(T). The turbulence in terms of std(V) is increasing throughout the flow with increasing y. For y/L = 0.1, 0.3 and 0.5, the profiles of std(V) has two peaks that coincide with the maximum velocity gradients in the mean velocity profile as expected. The peaks reflect the production of turbulence due to the velocity profile of the plume. The standard deviation of the temperature std(T) is high (about 1°C) throughout the domain, except for the distinct peak at y/L=0.1 just above the heat plate. The high value can be explained by hot fluid parcels rising from the heated plate. These hot fluid parcels can be observed in instantaneous temperature maps as shown in figure 5. The main contribution to the standard deviation is taken to be measurement noise in the recording process and noise due to pulse-to-pulse variations in laser light intensity.

Finally, figure 8 shows two components of the Reynolds flux vector, which is also shown as a vector plot in figure 9. Reynolds fluxes are only significant in the plume region. The main component is the vertical $\overline{v'T'}$-component in the y-direction and it is positive upwards, i.e. towards increasing temperature. This Reynolds flux component probably primary relates to hot fluid parcels moving upwards driven by the buoyancy force. For y/L = 0.1 and 0.3 there is a sharp peak in $\overline{v'T'}$ at x/L = 0.06 and a second smaller peak for negative x. These peaks might be related to spots on the heated plate from which hot fluid is primarily rising. This would also explain the asymmetry in the velocity and temperature mean profiles for low values of y. Slightly negative values of $\overline{v'T'}$ are found at the edges of the plume. This indicates that downwards heat transport is found here in the stratified temperature field. The $\overline{v'T'}$-component is about 5 times larger than the $\overline{u'T'}$-component in the x-direction, which transports heat from the plume to the stratified layers of bulk fluid. This transport has the highest levels for y/L = 0.3 and 0.5.

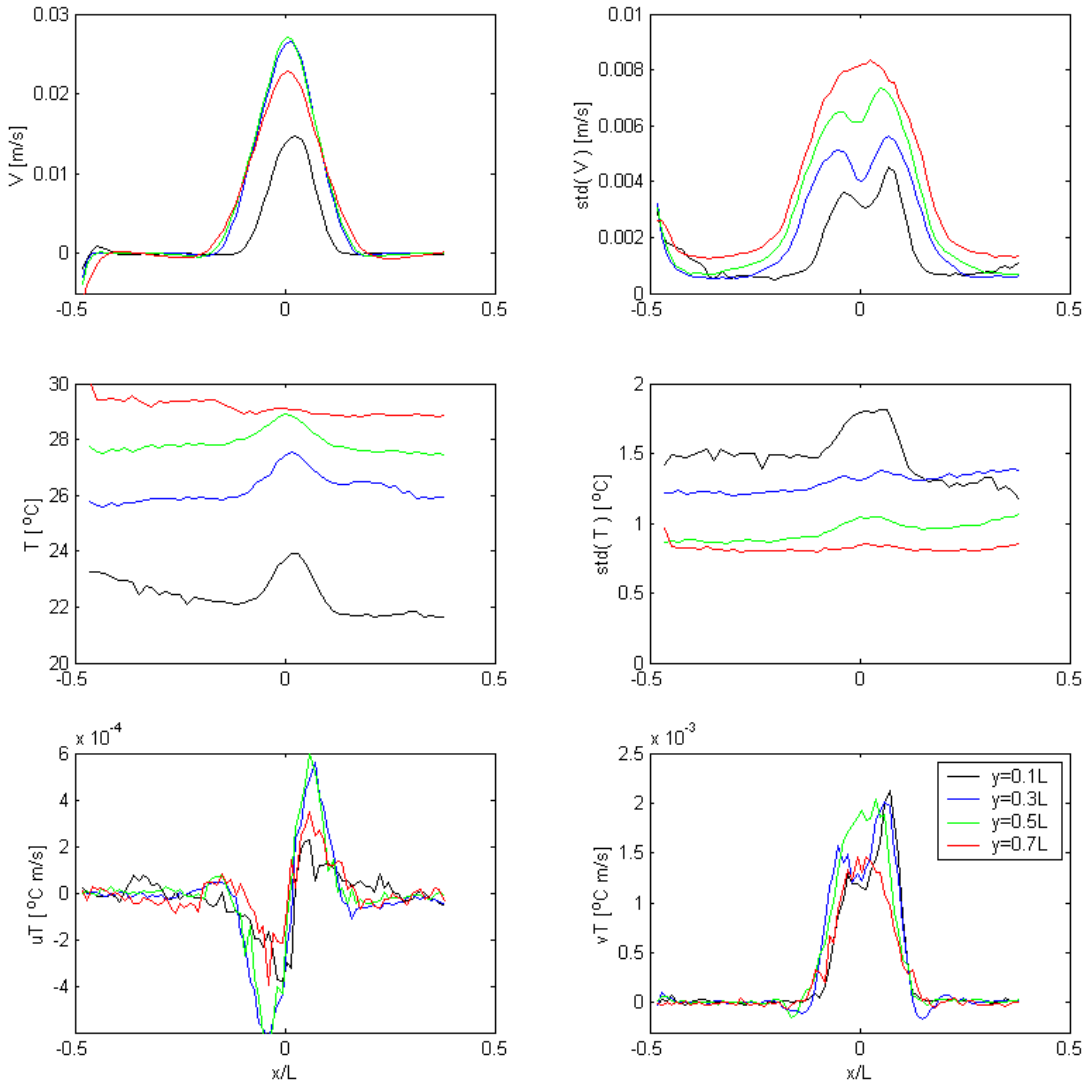

Fig. 8. Profiles of vertical mean velocity and its standard deviation, mean temperature and its standard deviation, horizontal and vertical Reynolds fluxes versus x/L for y/L = 0.1, 0.3, 0.5 and 0.7:

5. CONCLUSIONS

The paper presents simultaneous measurements of velocity and temperature by combined PIV and planar-LIF for a thermal plume in a square cavity. The results show that the flow consists of a plume rising in almost stagnant surrounding bulk fluid, having a stably stratified temperature field. The plume seems to be developed at a height above the bottom that is equal to about half the side length of the heated plate. Small downward velocities at the side of the plume are found at a height of 0.7 cavity side length above the bottom indicating that the presence of the top wall influences the flow at this position and that vortices are formed here.

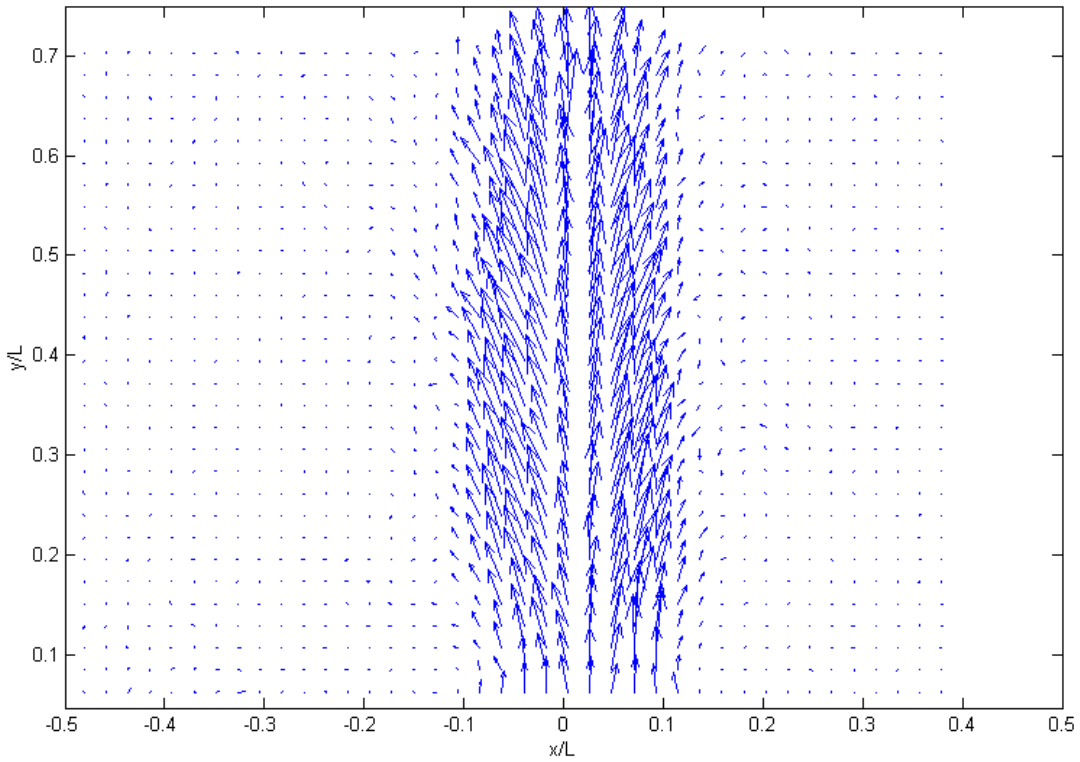

Fig. 9. Local Reynolds flux vectors ($\overline{u'T'}, \overline{v'T'}$) at every second location.

The measured Reynolds fluxes show that the dominating heat transport is in the plume in vertical upward direction. This transport is related to hot parcels of fluid rising due to buoyancy. There is also a considerable heat transport in horizontal direction from the plume to the surrounding stagnant fluid. This transports maintains the stably stratified temperature field found here. The turbulence intensity in terms of the standard deviation of vertical velocity has two peaks that coincide with locations of high velocity gradients, suggesting that a significant part of the turbulence is generated by the shear layers at the edges of the plume.

The flow is slightly asymmetric near the heated plate. The asymmetry is found both in vertical mean velocity and Reynolds flux. It is not clear whether this is caused asymmetries in the flow equipment or is a feature of the flow. This will be checked when experiments are repeated.

The interpretation of instantaneous temperature maps is limited by local pulse-to-pulse variations in the laser sheet. These variations cause changes in registered light intensity that have the same order of magnitude as local temperature variations. From the 1 Hz record of raw images the thermal structures in the plume can be followed by the eye because the human eye is used to correct for shadows. After conversion to temperature, the thermal structures are more difficult to follow. This is due to variations between laser pulses and beam profile in each pulse. This was not corrected for in the present study. The data suggest that it is possible to reduce the effect of this error significantly by using a vertical reference line in a region with low temperature variations. In this case it could be a line in the stagnant fluid region. It is expected that the accuracy of instantaneous temperature maps could be improved to a level of better than 0.5°C.

The present study has been used to employ combined PIV/planar-LIF in natural convection. We plan to do more detailed measurements with improved accuracy of the temperature. The measurements can be extended to cover more planes in the cavity. It will also be interesting to zoom in to regions like the heated plate and the sidewall boundary layers. Further, it will be interesting to do an analysis of flow structures and flow dynamics in order to improve the understanding of turbulent natural convection in confined spaces. Finally, the data are well suited for test of numerical calculations and the performance of turbulence models for a natural convection flow.

REFERENCES

Coolen M.C.J., Kieft R.N., Rindt C.C.M. and Van Steenhoven A.A. (1999): “Application of 2-D LIF temperature measurements in water using a Nd:YAG laser” *Exp. Fluids* 27, 420-426

Guillard F., Trägårdh C. and Fuchs L. (2000): "A study of turbulent mixing in a turbine-agitated tank using a fluorescence technique" *Exp. Fluids* 28, 225-235

Incropera, F. P. and DeWitt, D. P. (1985): “Fundamentals of heat and mass transfer”, 2nd edition, Wiley.

Leong, W. H., Hollands, K. G. T. and Brunger, A. P. (1999): “Experimental Nusselt numbers for a cubical-cavity benchmark problem in natural convection”, *Int. J. Heat Mass Transfer*, 42, pp. 1979-1989,

Mahouast M. (1993): “Mesure des champs de concentration et de temperature dans un reacteur agité par traitement des images de la fluorescence induite par nappe laser” *Récent progrès en Génie des Procédés* 7, 53-60 (in French)

Meyer, K. E., Özcan, O., Larsen, P. S., Gjelstrup, P., Westergaard, C. H. (2000): “Point and planar LIF for velocity-concentration correlations in a jet in cross flow”, Proceedings of 10th International Symposium on Applications of Laser Techniques to Fluid Mechanics, Lisbon, 10-13 July, (Paper 18.5).

Seuntiëns, H. J., Kieft, R. N., Rindt, C. C. M. and van Steenhoven, A. A. (2001): “2D temperature measurements in the wake of a heated cylinder using LIF”, *Exp. Fluids*, 31, pp. 588-595.